2009

The TATA-Binding Protein Core Domain in Solution Variably Bends TATA Sequences via a Three-Step Binding Mechanism [tables & figures]

Roberto F. Delgadillo
University of Nebraska - Lincoln

JoDell E. Whittington
University of Nebraska - Lincoln

Laura K. Parkhurst
University of Nebraska - Lincoln

Lawrence J. Parkhurst
University of Nebraska - Lincoln, lparkhurst1@unl.edu

Published in *Biochemistry* 48 (2009), pp 1801–1809; doi: 10.1021/bi8018724

The work was supported by NIH Grants GM59346 and RR015468.

The TATA-Binding Protein Core Domain in Solution Variably Bends TATA Sequences via a Three-Step Binding Mechanism

Roberto F. Delgadillo, JoDell E. Whittington, Laura K. Parkhurst, and Lawrence J. Parkhurst

Department of Chemistry, University of Nebraska–Lincoln, Lincoln, Nebraska 68588-0304

Corresponding author — L. J. Parkhurst, tel 402 472-3316, fax 402 472-2044, e-mail lparkhurst1@unl.edu

Abstract

Studies of the binding and bending of the AdMLP TATA sequence (TATAAAAG) by the core domain of yeast TBP allow quantitation of the roles of the N-terminal domains of yeast and human TBP. All three proteins bind DNA via a three-step mechanism with no evidence for an initially bound but unbent DNA. The large enthalpy and entropy of activation for the first step in ***y***TBP binding can now be assigned to movement of the NTD from the DNA binding pocket and not to energetics of DNA bending. The energetic patterns for ***h***TBP and ***c***TBP suggest that the 158-amino acid NTD in ***h***TBP does not initially occupy the DNA binding pocket. Despite the appearance of similar energetics for ***h***TBP and ***c***TBP, order of magnitude differences in rate constants lead to differing populations of intermediates during DNA binding. We find that the NTDs destabilize the three bound forms of DNA for both ***y***TBP and ***h***TBP. For all three proteins, the DNA bend angle (θ) depends on the TATA sequence, with θ for ***c***TBP and ***h***TBP being greater than that for ***y***TBP. For all three proteins, θ for the G6 variant (TATAAGAG) varies with temperature and increases in the presence of osmolyte to be similar to that of AdMLP. Crystallographic studies of ***c***TBP binding to a number of variants had shown no dependence of DNA bending on sequence. The results reported here reveal a clear structural difference for the bound DNA in solution versus the crystal; we attribute the difference to the presence of osmolytes in the crystals.

Abbreviations

TBP	TATA-binding protein with ***c***, ***y***, and ***h*** denoting core, yeast, and human, respectively
AdMLP	adenovirus major late promoter
PIC	preinitiation complex
CTD	COOH-terminal domain
NTD	NH_2-terminal domain
FRET	fluorescence resonance energy transfer
T	TAMRA or *N*,*N*,*N*′,*N*′-tetramethyl-6-carboxyrhodamine
Xr	x-rhodamine
F	fluorescein
Xr(T)*AdMLP$_{dpx}$*F	14 bp DNA duplex (5′-CGCTATAAAAGGGC-3′) bearing the 8 bp AdMLP TATA sequence, with 5′-Xr or T and 3′-F on the top strand
°AdMLP$_{dpx}$°	unlabeled 14 bp DNA duplex

Table 1. Optimal Rate Constants at 25 °C and Corresponding Enthalpy and Entropy Profiles for ***c***TBP−DNA_{AdMLP} Reaction Steps [a]

	k_i [b]	$\Delta H_i^{\circ\ddagger}$ (kcal/mol)	$\Delta S_i^{\circ\ddagger}$ (cal K^{-1} mol^{-1}) [c]
$i = 1$	1.64 [1.58,1.70]	9.1 [8.5,9.7]	−1.56
$i = 2$	0.028 [0.020,0.040]	4.6 [2.0,7.7]	−52.2
$i = 3$	5.4 [4.25,6.55]	5.8 [2.8,9.1]	−37.4
$i = 4$	3.6 [3.02,4.26]	3.1 [1.1,5.1]	−47.5
$i = 5$	0.083 [0.063,0.104]	24.5 [21.1,28.0]	16.7
$i = 6$	0.007 [0.006,0.008]	3.1 [1.7,4.5]	−60
QYI_1	0.55 [0.48,0.62]		
QYI_2	0.51 [0.46,0.56]		
QY_{final}	0.506 [0.50,0.51]		

a The values shown are for 25 °C and 1 M standard state and assume $\Delta C_p^{\ddagger} = 0$ for a temperature independence for $\Delta H_i^{\circ\ddagger}$ or $\Delta S_i^{\circ\ddagger}$ in each reaction step *i*. The reported parameter error estimates are averages of those obtained from the variance matrix and simulated noise data fitting. The 15 × 15 variance matrix was calculated as described in ref 7 with the exception that 12 kinetics curves were used (nine stopped-flow association curves and three dissociation curves). Twenty simulated noisy data sets were created by adding random noise of the same magnitude as in the experimental data to obtain the distribution of fitted parameters (49).

b k_1 is a bimolecular rate constant with dimensions of μM^{-1} s^{-1}; the dimensions for k_2–k_6 are s^{-1}.

c $\Delta S_i^{\circ\ddagger}$ values were calculated with the transition-state theory with k_i and $\Delta H_i^{\circ\ddagger}$.

Table 2. Comparative Rate Constants for ***c***TBP, ***h***TBP, and ***y***TBP Corresponding to Equation 2 for 25 °C

	k_i (s^{-1}) [a]		
	*c*TBP	*h*TBP [b]	*y*TBP
$i = 1$	1.64 [1.58,1.70]	6.8 [6.4,6.9]	1.59 [1.56,1.66]
$i = 2$	0.028 [0.020,0.04]	3.0 [2.8,3.4]	0.118 [0.114,0.125]
$i = 3$	5.4 [4.25,6.55]	0.54 [0.51,0.57]	0.0288 [0.0283,0.0339]
$i = 4$	3.64 [3.02,4.26]	0.020 [0.015,0.025]	0.541 [0.534,1.01]
$i = 5$	0.083 [0.063,0.104]	0.096 [0.053,0.141]	0.365 [0.365,0.730]
$i = 6$	0.007 [0.006,0.008]	0.029 [0.024,0.034]	0.00354 [0.00349,0.00395]

a Rate constants shown are at 25 °C. k_1 is a bimolecular rate constant with dimensions of μM^{-1} s^{-1}.

b ***h***TBP data at 20 °C were used to calculate values at 25 °C from values for $\Delta H^{\circ\ddagger}$ (7).

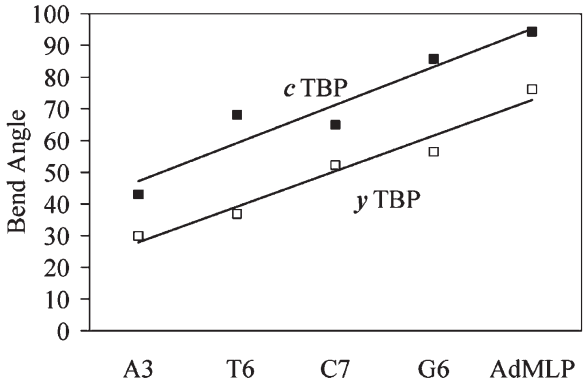

Figure 1. Broad range of bend angles induced in consensus and variant TATA sequences by the TBP core domain at 20 °C in solution. The filled squares represent data for ***c***TBP whereas the empty squares designate data for ***y***TBP (8), previously reported to have bend angles ranging from 29.9° to 76.2°.

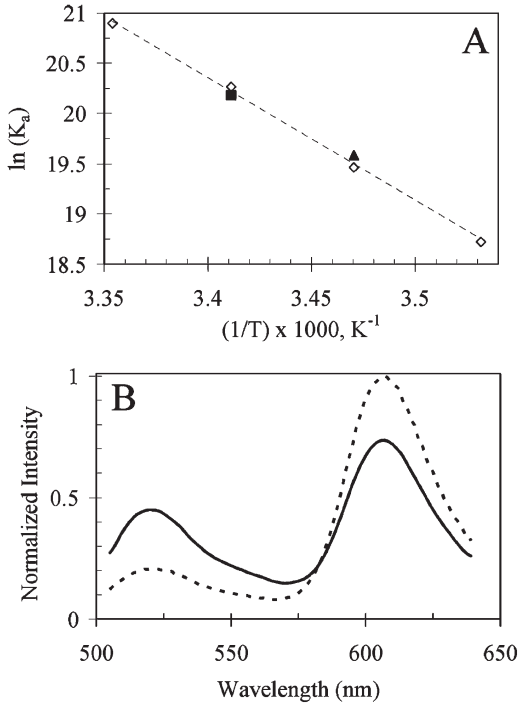

Figure 2. (A) van't Hoff plot of the combined ***c***TBP–DNA_{AdMLP} titration and temperature transition data. The K_a values obtained from the FRET (▲) and tyrosine (■) titrations together with those obtained from the temperature transitions (◊) were subjected to regression analysis to obtain the optimal values reported in the text at 10, 15, 20, and 25 °C. (B) Corresponding corrected emission spectra of unbound (——) and bound (- - -) xR*$AdMLP_{dpx}$*F are shown. The spectra of unbound and fully bound xR*$AdMLP_{dpx}$*F and of unbound and fully bound $AdMLP_{dpx}$*F are invariant over the experimental temperature range (4, 7).

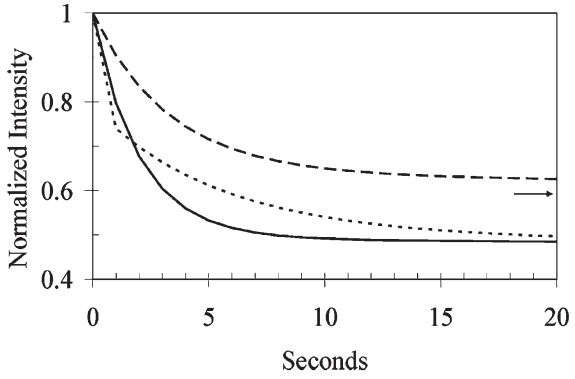

Figure 3. Theoretical stopped-flow FRET association curves calculated using the best fitting parameters derived from global fitting according to the three-step mechanism (4, 7). The curves are for 20 °C, with 20 nM DNA and 400 nM protein: ***c***TBP (——), ***h***TBP (···), and ***y***TBP (- - -). A biphasic profile is observed in each case with fluorescence changes of 42% for ***y***TBP and ~52% for ***h***TBP and ***c***TBP, which are proportional to the calculated bend angles of 77° and 95–97°, respectively. The arrow denotes the end point for the final very slow phase for ***y***TBP.

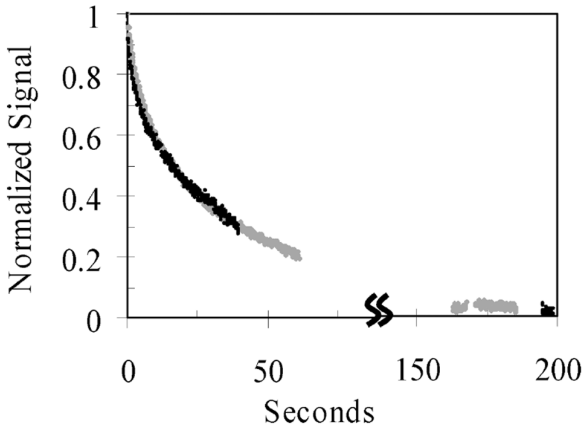

Figure 4. Comparison of the normalized observed raw stopped-flow FRET (gray points) and raw stopped-flow anisotropy (black points) association curves at 20 °C for 49 nM ***c***TBP. This experiment emphasized the first phase of the reaction. The excitation light beam was blocked during the time gaps in data collection to minimize photobleaching. The rates of the fast phases are identical within error: 0.34 ± 0.015 and 0.35 ± 0.02 s^{-1}, respectively. That these two experimental curves proceed at the same initial rate precludes a mechanism in which ***c***TBP binds to unbent DNA, as discussed in the text. Note that for both FRET and anisotropy, the normalized signal, $\hat{S}$, is $(S_t - S_\infty)/(S_0 - S_\infty)$; however, the FRET signal decreases with time, whereas the anisotropy increases with time.

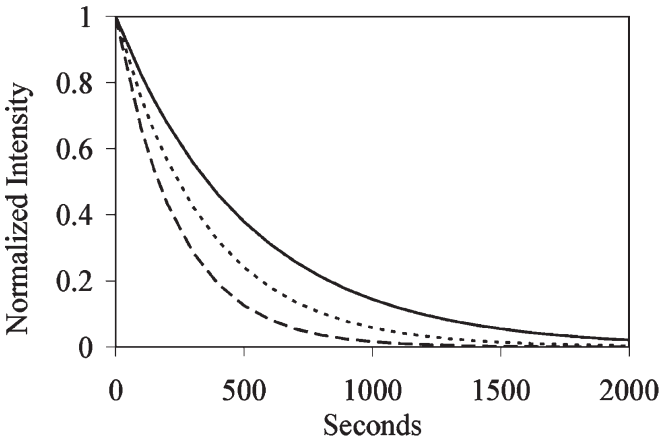

Figure 5. Measured relaxation rate for the replacement of labeled by unlabeled DNA_{AdMLP} in the equilibrated *c*TBP-xR*$AdMLP_{dpx}$*F complex, which was inversely dependent on temperature: 25 (——), 20 (···), and 15 °C (---) with corresponding monophasic decays of 0.0019 ± 0.0001, 0.0029 ± 0.0002, and 0.0042 ± 0.0002 s^{-1}, respectively.

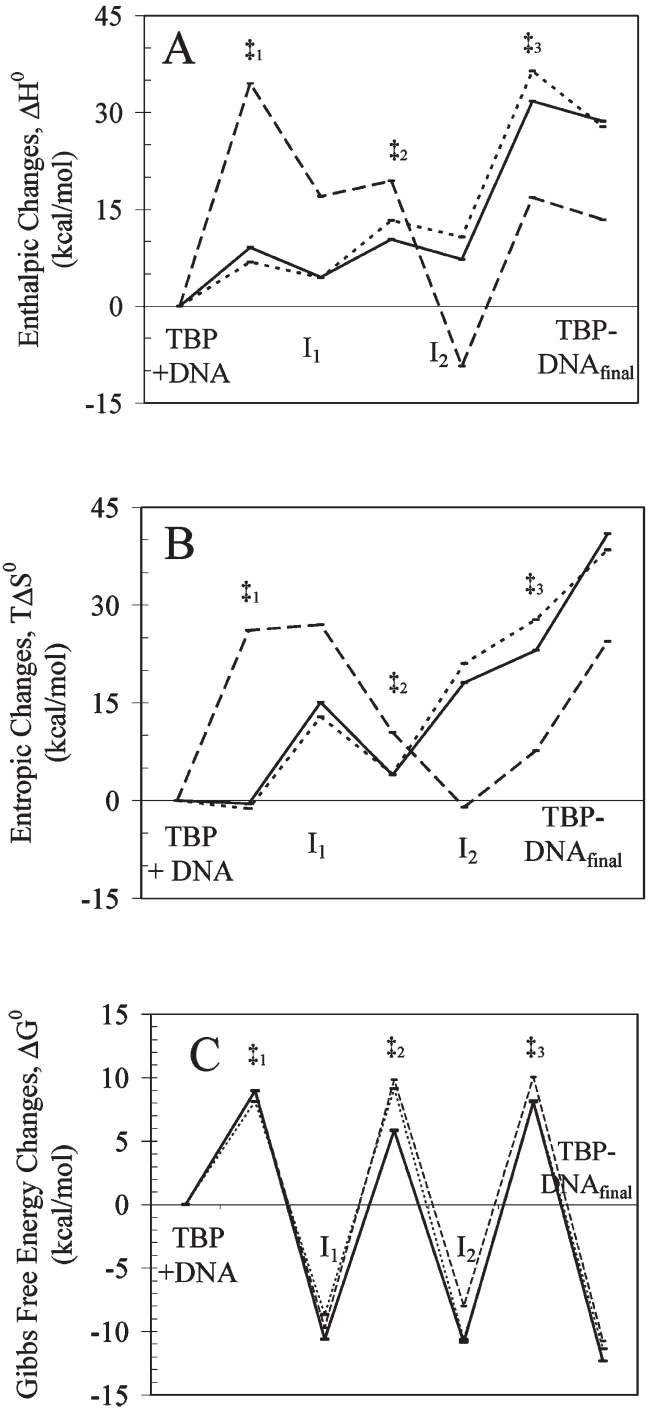

Figure 6. Thermodynamic profiles for *c*TBP, *h*TBP, and *y*TBP at 25 °C. The enthalpic progression of the reaction for the core (——), human (···), and yeast (---) proteins (A) and the corresponding entropic changes $T\Delta S^{\circ\ddagger}$ (B) and free energy change $\Delta G^{\circ\ddagger}$ (C) are shown. The $^{\ddagger}_{i}$ symbol denotes a transition state for step *i*. The *y*TBP reaction follows a markedly different energetic course than those of *c*TBP and *h*TBP, which have similar patterns.

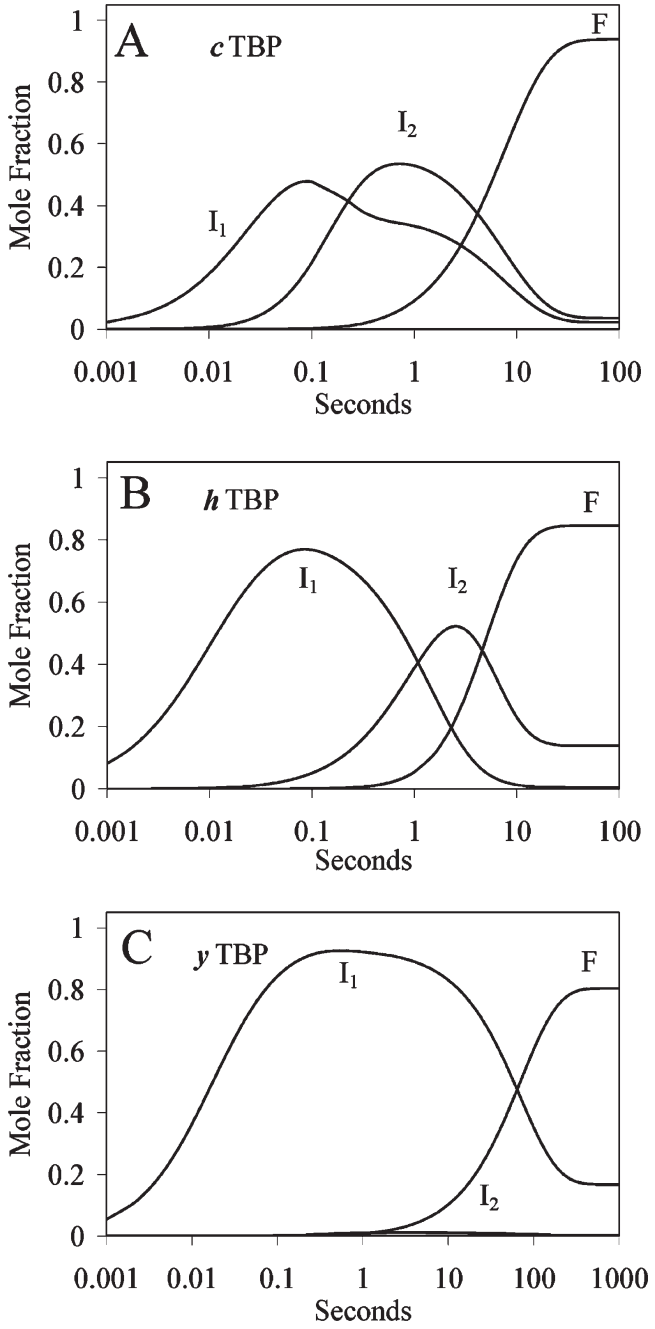

Figure 7. Time evolution of the reactive species for the *c*TBP–DNA_{AdMLP} reaction at 37 °C (A) for 10 μM protein and DNA. The dominance of $\mathbf{I_2}$ over $\mathbf{I_1}$ for *c*TBP distinguishes this reaction from those of *h*TBP [B (7)] and *y*TBP [C (4)], in which $\mathbf{I_1}$ prevails and remains present in the yeast reaction in significant mole fractions at equilibrium. At 37 °C, *y*TBP reaches equilibrium ~10 times more slowly than either *h*TBP or *c*TBP.